Journal of Energy Chemistry 104 (2025) 176–184

Contents lists available at ScienceDirect

Journal of Energy Chemistry

journal homepage: www.elsevier.com/locate/jechem

http://www.journals.elsevier.com/journal-of-energy-chemistry/

Regulating the mechano-electrochemistry of graphite-silicon hybrid anode through layered electrode structure design

Chunhao Li [a], Jing Wang [b], Xiancheng Wang [a], Zihe Chen [a], Renming Zhan [a], Xiangrui Duan [a], Xuerui Liu [a], Kai Cheng [a], Zhao Cai [b,*], Li Wang [c,*], Yongming Sun [a,*]

[a] Wuhan National Laboratory for Optoelectronics, Huazhong University of Science and Technology, Wuhan 430074, Hubei, China
[b] Faculty of Materials Science and Chemistry, China University of Geosciences, Wuhan 430074, Hubei, China
[c] Institute of Nuclear and New Energy Technology, Tsinghua University, Beijing 100084, China

ARTICLE INFO

Article history:
Received 1 December 2024
Revised 26 December 2024
Accepted 26 December 2024
Available online 8 January 2025

Keywords:
Graphite-silicon hybrid anode
Electrode structure
Mechano-electrochemistry
Local interfacial stress
Cycling stability

ABSTRACT

Graphite-silicon species (Gr-Si) hybrid anodes have merged as potential candidates for high-energy lithium-ion batteries (LIBs), yet long been plagued by rapid capacity fading due to their unstable mechano-electrochemistry. The dominant approach to enhance electrochemical stability of the Gr-Si hybrid anodes typically involves the optimization of the electrode material structures and the employment of low active Si species content in electrode (<10 wt% in most instances). However, the electrode structure design, a factor of equal importance in determining the electrochemical performance of Gr-Si hybrid anodes, has received scant attention. In this study, three Gr-Si hybrid anodes with the identical material composition but distinct electrode structures are designed to investigate the mechano-electrochemistry of the electrodes. It is revealed that the substantial volume change of Si species particles in Gr-Si hybrid anodes led to the local lattice stress of Gr at their contact interface during the charge/discharge processes, thereby increasing thermodynamic and kinetic barrier of Li-ion migration. Furthermore, the huge disparity in volume change of Si species and Gr particles trigger the separate agglomeration of these two materials, resulting in a considerable electrode volume change and increased electrochemical resistance. An advanced Gr/Si hybrid anode with upper Gr and lower Si species layer structure design addresses the above challenges using photovoltaic waste silicon sources under high Si species content (17 wt%) and areal capacity (2.0 mA h cm^{-2}) in Ah-level full pouch cells with a low negative/positive (N/P) ratio of 1.09. The cell shows stable cycling for 100 cycles at 0.3 *C* with an impressively low capacity decay rate of 0.0546% per cycle, outperforming most reported Gr-Si hybrid anodes.

1. Introduction

The rising of electric vehicle technology has simulated the rapid development of next-generation lithium-ion batteries (LIBs) with high energy density [1,2]. To date, Graphite (Gr) is the dominant anode material for commercial LIBs, while its low theoretical capacity (372 mA h g^{-1}) cannot satisfy the increasing demand on battery energy density [3–5]. Silicon (Si) species is a promising anode material with an order of magnitude higher theoretical Li-ion storage capacity (3579 mA h g^{-1} based on the lithiation product of $Li_{15}Si_4$), however, the drastic volume change and severe side reactions during charge/discharge processes have decreased the cycling stability of Si-based anodes and restricted their actual applications [6,7]. To make the trade-off between the capacity and cycling stability in a practical way, Gr-Si hybrid anodes with 3–10 wt% Si have been widely developed for commercial LIBs in recent years [8]. For instance, the 3.5 wt% Gr-Si anode showed a constant electrode thickness but significantly improved energy density from 135 Wh kg^{-1} to 180 Wh kg^{-1} on a cell level [9]. However, developing advanced Gr-Si hybrid anodes with high Si loading (>10 wt%) and long-term stability is still a grand challenge.

In principle, the electrochemical performance of an electrode is determined by two critical factors: Materials that make up the electrodes and structures that integrate each material [10–12]. To improve the cycling stability of Gr-Si hybrid electrodes, a number of material design strategies including: (1) constructing a Si

* Corresponding authors.
E-mail addresses: caizhao@cug.edu.cn (Z. Cai), wang-l@tsinghua.edu.cn (L. Wang), yongmingsun@hust.edu.cn (Y. Sun).

https://doi.org/10.1016/j.jechem.2024.12.048

surface layer on Gr particles [13–20], (2) nano-sizing Gr and Si materials [21–26], (3) surface oxidation state control of Si [27,28], and (4) binder design to enhance Gr-Si connection [29–31], have been proposed. These studies have focused on the modification of Gr or Si materials and have showed success in developing cycle-stable Gr-Si hybrid anodes [13,23,25]. However, these approaches often entail intricate or energy-intensive synthesis processes, which posed a great challenge for the large-scale preparation of materials as well as the subsequent application. To date, the other key factor (i.e., electrode structures) that jointly decides the electrode performance has rarely been studied. More importantly, the cycling stability of Gr-Si hybrid anodes is even worse than the mono-component Si or Gr counterparts [32], implying that the interaction between Si and Gr materials plays a significant role on the cycling stability, which could be optimized by a structural design within the electrode. Therefore, it's vital to uncover the interplay between Si and Gr material during battery cycling and optimize the electrode structure for designing advanced Gr-Si hybrid anode with long-term cycling stability.

Gr-Si hybrid anodes with 3–10 wt% Si have been widely studied [19,23]. However, the structure-capacity relationship of Gr-Si hybrid anodes has rarely been reported. In this work, three Gr-Si hybrid anodes with identical material compositions with 5 wt% Si among this range (3–10 wt% Si) but distinct electrode structures were fabricated and studied to elucidate the mechano-electrochemical interactions within the electrodes, including a conventional Gr-Si hybrid electrode structure with random particle distribution (conventional Gr-Si), a layered electrode structure with Gr particle layer enveloped by a Si particle layer (layered Si/Gr), and a layered electrode structure with Si particle layer enveloped by a Gr particle layer (layered Gr/Si). It was revealed that the substantial volume expansion of Si particles exerted a local lattice stress of Gr, resulting in the severe capacity fading of Gr in the conventional Gr-Si electrode. Moreover, the disparate volume change of Si and Gr particles resulted in the separate agglomeration of Si and Gr particles, and the subsequent formation of porous electrode structure, which was detrimental to the smooth charge transfer and stable cycling performance. Consequently, the layered Gr/Si electrode, characterized by the minimal Si/Gr interface and the most stable electrode structure, exhibited the highest average Coulombic efficiency (ACE) of 99.2%. Additionally, it demonstrated exhibited a stable cycling performance with 94.4% capacity retention in layered Gr/Si||Li half cells after 100 cycles at 0.2 *C*. This performance was markedly superior to the conventional Gr-Si counterpart with only a capacity retention of 46.6% under the same test condition. Furthermore, the efficacy of the layered Gr/Si hybrid electrode with a high photovoltaic waste Si loading (17 wt%), was also substantiated in an Ah-level pouch cell with a low negative/-positive (N/P) ratio of 1.09. This configuration exhibited stable cycling for over 100 cycles at the slow rate of 0.3 *C*, with an exceptional capacity decay rate of 0.0546% per cycle. Our work not only illuminated the mechano-electrochemical instability issue of conventional Gr-Si hybrid electrodes, but also offered a novel perspective on the development of advanced Gr-Si hybrid anodes by meticulous electrode structure design. The as-demonstrated electrode structure design demonstrated in this work opened up a new way for the development of next-generation LIBs with high energy density and long lifespan.

2. Experimental

2.1. Electrode preparation

Si photovoltaic waste from Golden Concord Holdings Limited was employed as the Si powder active materials and treated with a ball-milling before use. The milling process was conducted at 350 r min^{-1} for 15 h (2 min off every 10 min) at a ball-to-powder weight of 12:1. Commercial Gr and nanoSi powder was purchased from Kluthe Chemical (Shanghai) Co., Ltd. The SiO_x was prepared by annealing Si photovoltaic waste at 600 °C for 2 h. The Li polyacrylic acid (LiPAA) binder was purchased from Canrd Co., Ltd. The Gr-Si electrode (Si:Gr = 5:95 or 17:83 wt%) were fabricated by mixing the fixed mass ratio of Gr, Si, carbon black and LiPAA and pasting onto Cu foil. The mass loading of Gr and Si was calculated by multiplying mass loading of Gr-Si electrode by respective mass ratio. The layered Gr/Si electrodes (Si:Gr = 5:95 or 17:83 wt%) were fabricated by coating a Si layer and then a Gr layer on a copper foil (~20 μm), successively. The coating thickness of blade coater was adjusted to get the same mass loading of Si and Gr as Gr-Si electrode. For electrodes with 95 wt% Gr and 5 wt% Si, the active material loading is ~6.38 mg cm^{-2}. For electrodes with 83 wt% Gr and 17 wt% Si, the active material loading is ~3.59 mg cm^{-2}. Typically, Si particles, carbon black and LiPAA was mixed with a mass ratio of 8:1:1 to prepare a homogenous slurry, which was pasted onto a Cu foil and dried at room temperature. Gr slurry consisting of 90 wt% Gr particle, 5 wt% carbon black, and 5 wt% LiPAA was then pasted onto the above obtained Si electrode, and dried at 80 °C overnight. Similarly, layered Si/Gr electrodes were fabricated by coating the Gr layer on a copper foil first and the Si layer then.

2.2. Structural characterization

The morphology and elemental distribution of the electrodes were characterized via a Nova NanoSEM 450 microscope. X-ray diffraction (XRD) analysis was carried out on a PANalytical B.V. Empyrean X-ray diffractometer (Cu K_α radiation, 40 kV, 30 mA). Raman measurement was performed on a WITec Alpha300 R Raman imaging instrument with 532 nm excitation. Electron probe micro-analysis (EPMA) characterization was conducted on a Shimadzu EPMA-8050G electron probe microanalyzer.

2.3. Electrochemical testing

The electrochemical performance of the electrode was analysed with a LANDT battery tester using half coin cells and full pouch cells. The half cells were assembled using standard 2032-type coin cells with a lithium foil counter electrode and an electrolyte of 1.2 M $LiPF_6$ dissolved in a mixture of ethylene carbonate (EC), ethyl methyl carbonate (EMC) and dimethyl carbonate (DMC) (1:1:1 in volume) with 10 vol% fluoroethylene carbonate (FEC) as an additive. Celgard 2300 (19 μm, PP/PE/PP) was adopted as the separator. The pouch full cells were assembled with Gr-SiO_x anodes (prepared with the same procedure as that for Gr-Si except using SiO_x instead of Si), commercial NCM622 cathodes (areal capacity: 2.0 mA h cm^{-2}, Shanshan Co., Ltd.), and the same electrolyte as that employed in half cells. Prelithiation process was carried out for Gr-SiO_x hybrid electrode and layered Gr/SiO_x in half pouch cells, which were first discharged to 0.01 V, and then charged to 1 V. After that, the full cells were assembled by coupling the prelithiated anodes and commercial NCM622 cathodes. The full cells were first activated for 5 electrochemical cycles at 0.1 *C*, then charged at a constant current of 0.3 *C* to 4.2 V, followed by a constant voltage charging process at 4.2 V to 0.1 *C* and a constant current discharging process at 0.3 *C* to 2.8 V. Electrochemical impedance spectroscopy (EIS) was performed in half cells with Li foil as reference electrode, and tested on a Biologic VPM3 electrochemical station at open circuit voltage and an alternating current (AC) voltage of 5 mV from 0.1 to 100000 Hz. Lithium-ion diffusion coefficient of conventional Gr-Si, layered Si/Gr, and layered Gr/Si electrodes after cycling was calculated from the inclined line in the low-frequency region by the following equation: $D = R^2T^2/2A^2n^4F^4C^2s_w^2$, where, s_w is the

Warburg impedance coefficient. R, T, and A denote the gas constant, operating temperature, and electrode area, respectively. n, F, and C signify the number of electrons per molecule, Faraday constant, and molar concentration of Li ion, respectively.

2.4. Calculation methods

All calculations were carried out using density functional theory with the Perdew-Burke-Ernzerhof's exchange–correlation functional as implemented in the Vienna ab initio simulation package. The core electrons of atoms were described with a projected augmented wave method, while the valence electrons were represented with a planewave basis set with a cut-off energy of 400 eV. The bulk lattice constants were optimized using the 2 × 2 × 1 Monkhorst-Pack k-point sampling. The Gibbs free-energy (ΔG_{Li+}) of Li-ion diffusion in different layer space graphite was calculated by the following equations: $\Delta G_{Li+} = \Delta G_{Li\text{-}C} - \Delta G_{Li} - \Delta G_C$, where $\Delta G_{Li\text{-}C}$ was the free energy of a lithium ion embedded in graphite, and the ΔG_{Li} and ΔG_C stand for the free energy of a lithium ion and graphite. The migration pathways of lithium ion between graphite layers were broken into a series of elementary processes, for each of which the transition-state structure was obtained using the nudged-elastic-band method. Between reactant and product, six imaged were generated to achieve smooth energy curve with a force tolerance of 0.01 eV $Å^{-3}$.

3. Results and discussion

To understand the structure-capacity relationship of Gr-Si hybrid anodes, conventional Gr-Si, layered Si/Gr, and layered Si/Gr electrodes with the same material composition (95 wt% Gr and 5 wt% Si) and different electrode structures were designed and fabricated (Fig. 1a). These electrodes were paired with metallic Li foil counter electrodes and tested in the half cells cycling at 0.2 C. As shown in the Fig. 1b, the layered Gr/Si electrode showed a high capacity retention of 92.7% after 100 cycles, superior than the conventional Gr-Si (81.9%) and layered Si/Gr electrodes (85.7%). Moreover, the ACE of the layered Gr/Si electrode (99.7%) was much higher than that of the conventional Gr-Si (99.3%) and layered Si/Gr electrodes (99.5%), suggesting the highest cycling stability of the layered Gr/Si electrode. The charge/discharge curves of the layered Si/Gr and layered Gr/Si electrodes were nearly overlapped with the conventional Gr-Si electrode, suggesting that layered electrodes had the same reaction kinetics and (de)lithiation behaviour as the hybrid one (Fig. 1c). However, they displayed different degrees of capacity fading after 100 electrochemical cycles (Fig. 1d). Since the Li^+ ion extraction of Gr-Si hybrid electrodes occurs preferentially from Gr at 0.01–0.23 V and subsequently from Si at 0.23–1.0 V [33], the capacity contribution of Gr and Si components of the three electrodes were deconvoluted and compared in order to understand such diverse cycling performance (Fig. 1e, f). The detail and example of data processing procedure is shown in the Table S1. It was noted that the capacity retention of Gr in conventional Gr-Si electrode (91.6%) was much lower than that in the layered Si/Gr (96.2%) and Gr/Si (99.7%) electrodes, implying the interface between Gr and Si had a negative effect on the stable performance of Gr. Moreover, the Gr materials in conventional Gr-Si electrode with 5 wt% Si exhibited a discharge capacity of 310 mA h g^{-1} at the 1st cycle, and capacity retention of 99.2%, 96.4%, 91.6% for the 10th, 50th, and 100th cycles, respectively (Fig. 1e). The differential capacity plots in Fig. S1 revealed three characteristic delithiation peaks of Gr at 0.11, 0.16, and 0.23 V vs. Li/Li^+, which shifted towards higher voltages for the conventional Gr-Si electrode after cycling, suggesting that the Li-ion migration in the interlayers of Gr turned to be unfavorable. In addition, the Si materials in the electrode exhibited a discharge capacity of 2552 mA h g^{-1} at the 1st cycle, and capacity retention of 95.3%, 75.2%, 60.2% for the 10th, 50th, and 100th cycles, respectively (Fig. 1f). The capacity retention of Si in the layered Gr/Si electrode (82.8%) was much higher than that in the layered Si/Gr (66.8%) and conventional Gr-Si (60.2%) electrodes, implying the less contact between Si and electrolyte would be beneficial for the cycling stability of Gr-Si hybrid electrode. The rate performance of these three electrodes was also provided. As shown in Fig. S2, at 0.25 C, both three electrodes demonstrate comparable electrochemical performance. As the C rate increased to 0.5 and 1 C, layered Gr/Si electrode shows slightly higher specific capacity than conventional Gr-Si and layered Si/Gr. The layered Gr/Si electrode delivered better capacity retention over the extended cycle number at various C rates. It may be attributed to the graphite layer near electrolyte provides a good conductive network and good structural durability, enhancing the rate and stability of Gr/Si electrode.

To investigate the degradation of Gr material in the conventional Gr-Si hybrid electrode, XRD was first employed. As shown in Fig. 2a and Fig. S3a, the (002) diffraction peak of Gr shifted to lower degrees after 100 cycles, and accompanied by significant variations in intensity and full width at half-maximum, indicating that partial Li ions could not be deintercalated and disrupted lattice parameter [34]. The absent Si peaks in the XRD of Gr-Si electrode with 5 wt% Si may be resulted from its too low silicon content compared with that with 17 wt% Si (Fig. S3b). In addition, we noted that the color of conventional Gr-Si electrode was black before cycling, the same as pure Gr, but turned to dark yellow after cycling (Fig. 2b), such color was in agreement with the XRD that the Gr maintained a partial lithiated state after delithiation to 1 V [3]. Furthermore, *in-situ* optical and two-dimensional (2D) Raman tests of Gr/Si electrode were carried out and shown in Fig. S4. The two obvious peaks at 1340 and 1570 cm^{-1} could be assigned to defect-induced D band and in-plane vibrational G band from Gr, respectively (Fig. 2c). The D/G band peak intensity ratio (I_D/I_G) could be an indicator of the structural disorder degree of Gr [35,36]. Notably, The Gr in the Gr-Si electrode after 10 cycles showed substantially increased I_D/I_G ratio in the full detected area (40 μm × 40 μm) compared with that before cycling (Fig. S4a), revealing the deteriorative structural of Gr in the cycled conventional Gr-Si electrode. Moreover, the 2D Raman maps of the I_D/I_G ratio for the conventional Gr-Si electrode before and after 100 cycles were shown in Fig. 2d, and the Gr in the conventional Gr-Si electrode also showed hugely increased I_D/I_G ratio in the full detected area (100 μm × 50 μm), further confirming the severe structural disordering of Gr in the cycled conventional Gr-Si electrode. The large volume change of Si particles (i.e., >300%) would stress Gr at their contact interface, which could be responsible for the local stress and structural disordering of Gr in the conventional Gr-Si electrode after cycling, not conducive to the Li-ion intercalation and diffusion at Gr interlayers (Fig. 2e) [37]. The (002) diffraction peak of Gr in cycled layered Gr/Si and Si/Gr electrodes accorded with that of pristine Gr (Fig. S5a). Moreover, in contrast to the large I_D/I_G ratio of Gr in the cycled conventional Gr-Si electrode (0.98), the I_D/I_G ratio of Gr in the cycled layered Gr/Si and Si/Gr electrodes turned out to be 0.45 and 0.48, quite close to that of pristine Gr (0.39) (Figs. S4b and S5b). For better comparison, in-situ optical and 2D Raman tests of Gr/Si electrode were carried out (Fig. S4b). The Gr in the Gr/Si electrode after cycling showed slight increased I_D/I_G ratio in the full detected area compared with that before cycling. These results in turn substantiated that an abundance of contact interfaces between Gr and Si precipitated the performance degradation of Gr materials in conventional Gr-Si electrodes. To further validate the deterioration at the interface between expanded Si and Gr, the Li-ion migration

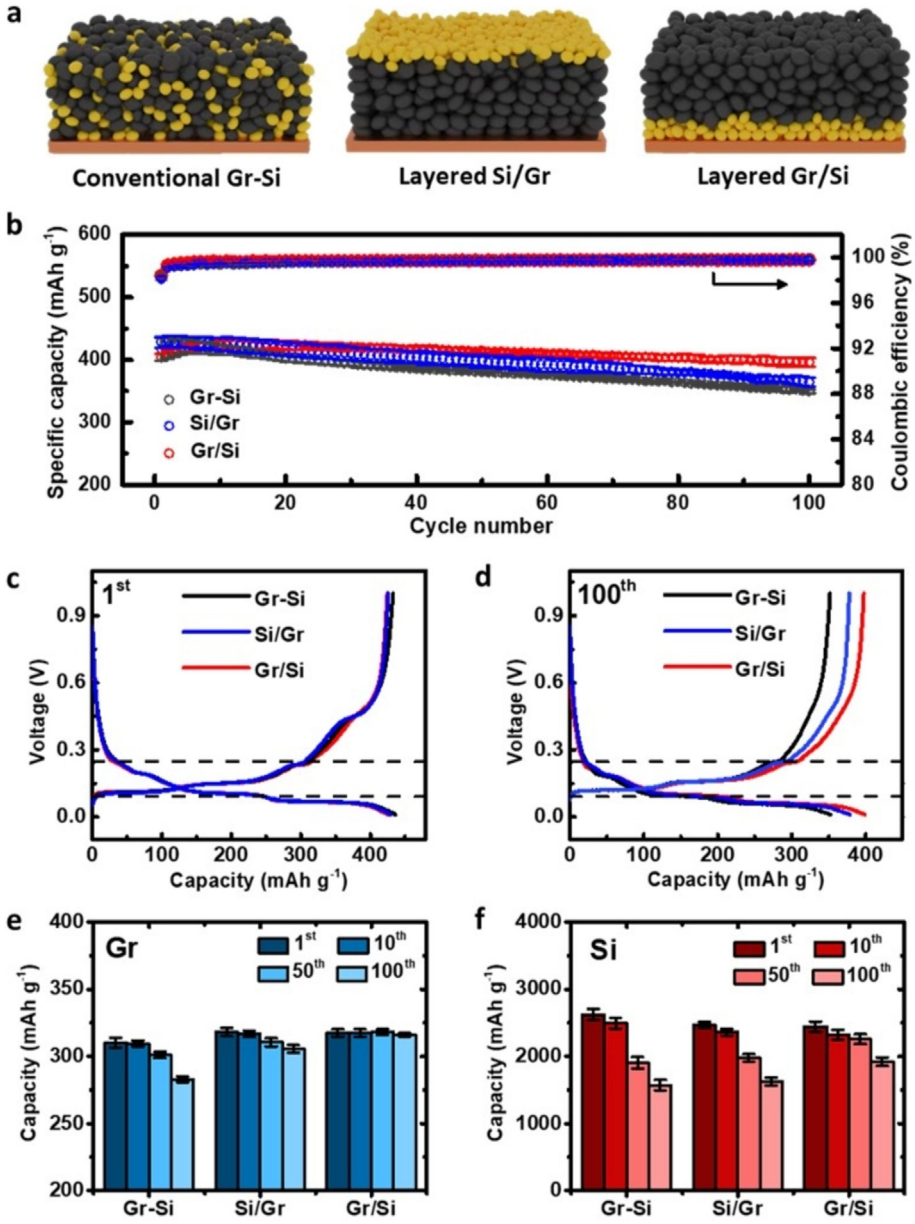

Fig. 1. (a) The schematic of the electrode structures of conventional Gr-Si, layered Si/Gr, and layered Gr/Si electrodes. The black balls and yellow balls represent Gr and Si, respectively. (b) Cycling performance and Coulombic efficiency of conventional Gr-Si||Li, layered Si/Gr||Li, and layered Gr/Si||Li half cells at 0.2 *C*. Charge and Discharge curves of conventional Gr-Si||Li, layered Si/Gr||Li, and layered Gr/Si||Li half cells for the (c) 1st and (d) 100th cycles. Capacity contributions of (e) Gr and (f) Si for the conventional Gr-Si, layered Si/Gr, and layered Gr/Si electrodes with 5 wt% Si loading at the 1st, 10th, 50th and 100th cycles.

thermodynamic and kinetics in the interlayers of stressed Gr was studied based on first principles calculation (Figs. S6 and S7). With an interfacial stress applied and 5% interlayer spacing reduced (from 0.3354 to 0.3186 nm), the Gibbs free energy for Li-ion intercalation increased from 0.86 to 1.11 eV (Fig. 2f). Furthermore, the energy barrier of Li-ion diffusion also turned higher (from 0.22 to 0.31 eV, Fig. 2g), reflecting the both worsen thermodynamic and kinetics for Li-ion storage in locally stressed Gr materials, in accord with the XRD results that Li-ion could not be fully deintercalated in cycled conventional Gr-Si electrode.

The electrode structure of the conventional Gr-Si anode before and after cycling was further examined by scanning electron microscope (SEM) and energy dispersive spectroscopy (EDS). As shown in Fig. 3a, the Gr and Si particles in the conventional Gr-Si anode before cycling was homogeneously mixed with a dense structure, the element distribution of Si and C was relatively uniform, the thickness of the electrode was determined to be 65.6 μm. After 100 cycles at 0.2 *C*, the Gr-Si anode turned to be loose and porous with an increased thickness of 131.8 μm, suggesting a high thickness/volume change ratio of 201%. Moreover, the EDS results suggested non-uniform distribution of Si and C elements, indicating that the huge difference in volume change of Si and Gr particles led to the separated agglomeration of Si and Gr particles. Such electrode structure evolution was also studied by EPMA. As demonstrated in Fig. 3b and Fig. S8, the conventional Gr-Si electrode before cycling showed a dense surface with uniform Si and Gr distribution. However, after 100 electrochemical cycles at 0.2 *C*, a number of cracks could be clearly observed on the surface of the conventional Gr-Si electrode (Fig. 3c and Fig. S9). Moreover, the C and Si mappings indicated the aggregation of Gr and Si particles after cycling. Notably, the Si was enriched at the surface of the conventional Gr-Si electrode after cycling, imply-

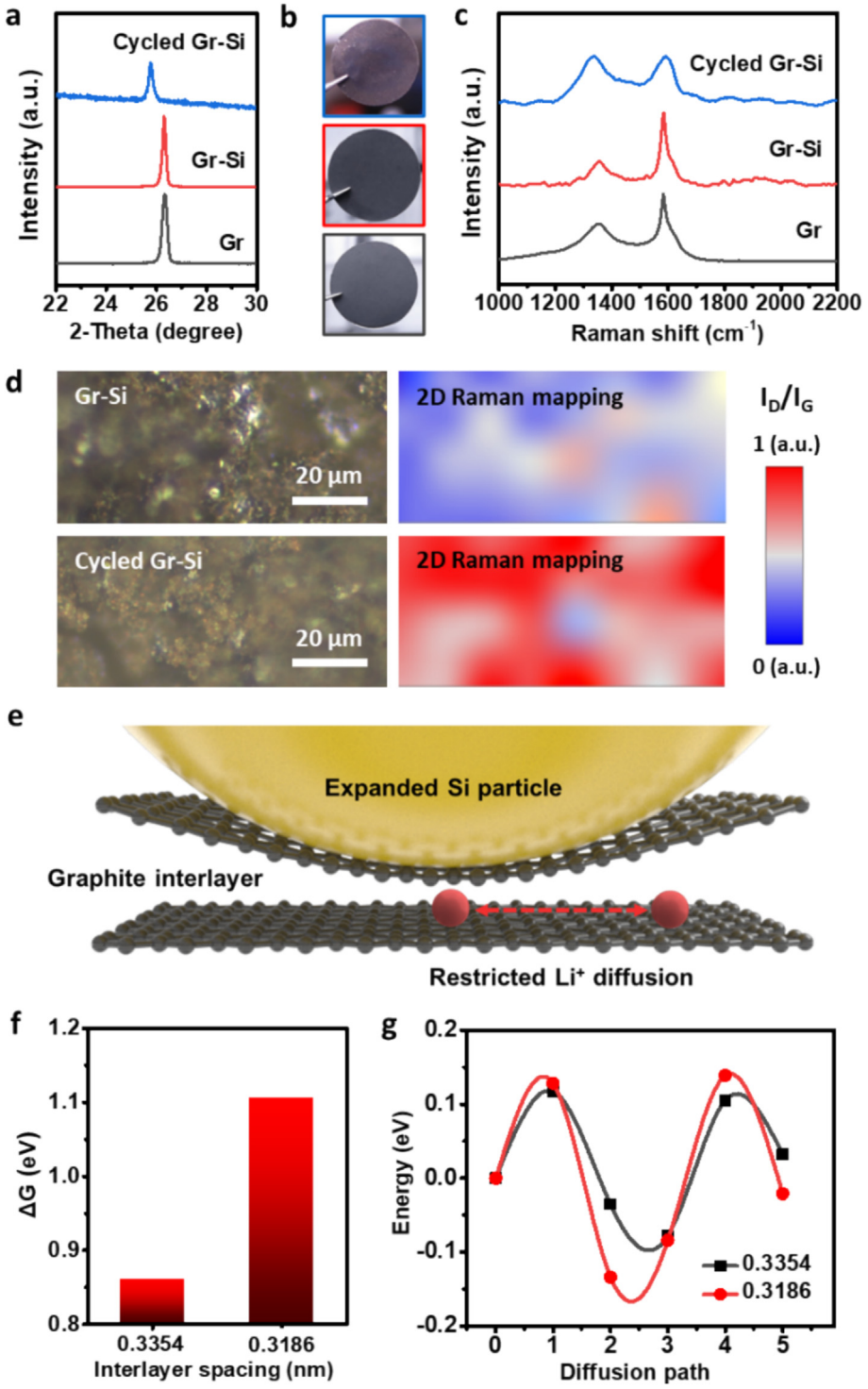

Fig. 2. (a) XRD patterns, (b) digital images, and (c) Raman spectra of the pure Gr, conventional Gr-Si, and conventional Gr-Si electrodes at delithiation state after cycling. (d) Optical and 2D Raman images of conventional Gr-Si electrode before and after cycling, suggesting the defective nature of Gr in conventional Gr-Si electrode after cycling. (e) The schematic of the local interfacial stress between expanded Si and Gr materials. (f) Thermodynamic and (g) dynamic calculation results of Li-ion migration in stressed graphite with different interlayer spacings.

ing the Si particles migration to the electrode surface during battery cycling, which led to the mechano-electrochemical instability. These results were all evidence for the migration of Gr and Si particles during cycling and the formation of porous electrode for the cycled conventional Gr-Si anode.

To get deeper insight into the structure evolution of the widely used conventional Gr-Si hybrid electrode, layered Si/Gr and Gr/Si electrodes were also characterized and analysed under the same test conditions. As shown in Fig. 4a, the layered Si/Gr electrode showed an electrode structure consisting of a Gr particle layer at the bottom and a Si particle layer at the top. The layered Si/Gr electrode before cycling showed a relatively dense and uniform surface consisting of Si sheet particles. After 100 electrochemical cycles, the surface of layered Si/Gr electrode turned to be loose and

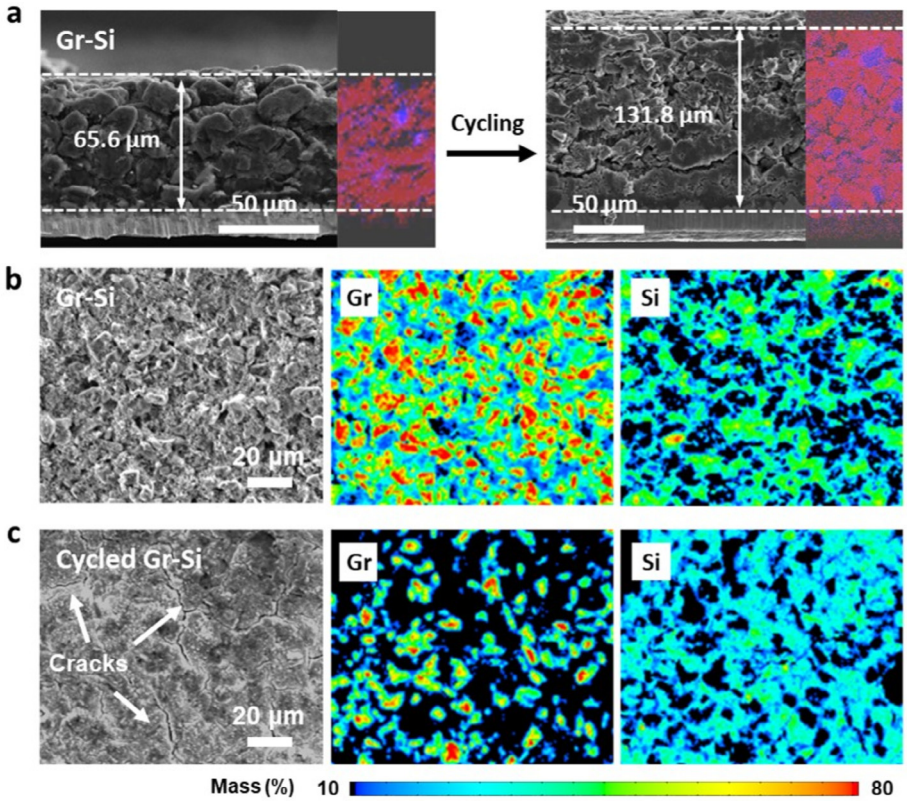

Fig. 3. (a) Cross-section SEM and EDS elemental mapping images of the conventional Gr-Si electrode before and after cycling at 0.2 *C* (the Si and C elements are displayed by blue and red, respectively). SEM and EPMA analysis of conventional Gr-Si electrode (b) before and (c) after cycling, suggesting that the different volume changes of Gr and Si particles led to the separate aggregation of Gr and Si particles and the formation of cracks after electrochemical cycling.

porous, with a number of cracks can be observed (Fig. S10). The thickness of the surface Si layer increased from 8.1 to 33.8 μm, indicating a significant thickness/volume change ratio of 417%. Long cracks could also be found in the cross-section image of the cycled layered Si/Gr electrode, indicating the severe side reactions of the surface Si particle layer, which should increase the charge transfer resistance and limit the electrode cycling lifespan. Conversely, under the same test conditions, the layered Gr/Si electrode after cycling showed the same dense and uniform surface morphology as that before cycling (Fig. S11). The thickness of the Si layer for the layered Gr/Si electrode demonstrated a thickness/volume change ratio of less than half (195%). Post-cycling, the Si layer of the layered Gr/Si electrode appeared relatively dense, with no significant crack observable (Fig. 4b), suggesting the most stable electrode structure. The large electrode volume change and the formation of porous electrode count against the stable electrochemical performance of the conventional Gr-Si electrode, which was studied by EIS. Before cycling, EIS curves of Gr/Si, Gr-Si and Si/Gr electrodes are similar, suggesting that initial charge transfer could not be impacted by electrode structure (Fig. S12). EIS of Gr-Si||Li, Si/Gr||Li, and Gr/Si||Li half cells after 5 and 100 electrochemical cycles were compared to analyze the evolution of interfacial property and electrode kinetics during cycling (Fig. 4c, d, Figs. S13 and S14), full details of the fitting results are shown in Table S2 in the Supporting Information. As shown in Table S2, Gr/Si electrode shows almost unchanged R_{ct} values after 5 and 100 cycles, while R_{ct} of Gr-Si and Si/Gr electrodes show significantly increase from the 5th to 100th cycles. In addition, lithium-ion diffusion coefficients for conventional Gr-Si, layered Si/Gr, and layered Gr/Si electrodes are 2.7×10^{-13}, 6.7×10^{-13} and 67×10^{-13} $cm^2\ s^{-1}$ after 100 cycles (Fig. S15). It suggested that layered Gr/Si electrode has the most stable structure, which can effectively reduce the interfacial impedance and facilitate the rapid transport of lithium-ion [38,39], in accord with the rate performance in Fig. S2. Moreover, Si/Gr electrodes exhibit the largest R_{SEI}, which may be due to more severe side reactions between upper Si and electrolyte than that in Gr-Si and Gr/Si electrode. In contrast, Gr/Si shows the lowest R_{SEI} values of 15.8 and 22.4 Ω cm^{-2} after 5 and 100 cycles, suggesting that the side-reactions of Si in the layered Gr/Si electrode could be largely suppressed during cycling, which should be beneficial for the electrochemical performance improvement.

Based on the above spectroscopic, theoretical, microscopic, and electrochemical analysis, a comprehensive understanding on the failure mechanism of the widely used conventional Gr-Si hybrid electrode was proposed (Fig. 4e). For conventional Gr-Si electrode, the large volume expansion of Si particle caused the local stress at the Gr/Si interface, leading to the deteriorated Li-ion storage performance. Moreover, the large difference in volume change of Si and Gr particles led to the agglomeration of Si and Gr particles separately, resulting in the formation of porous electrode, the increased charge transfer resistance, and the reduced cycling stability [40,41]. Reducing the contact interface should be beneficial for the cycling stability improvement of Gr-Si hybrid electrode. The layered Si/Gr electrode design has reduced the contact interfacial area between Gr and Si. However, the top Si components of Si/Gr electrodes experienced unrestricted volume expansion/contraction, which results in excessive thickening of the SEI. In contrast, the Gr layer on top of the Gr/Si electrode could apply a longitudinal force to mechanically restrict the SEI growth and the overall deformation [42]. In addition, SEI formed on graphite of Gr/Si electrode is thin due to its intrinsic small volume change. Therefore, the layered Gr/Si electrode with the minimum Gr/Si contact interfacial area and the most stable electrode structure should maintain the most stable cycling performance.

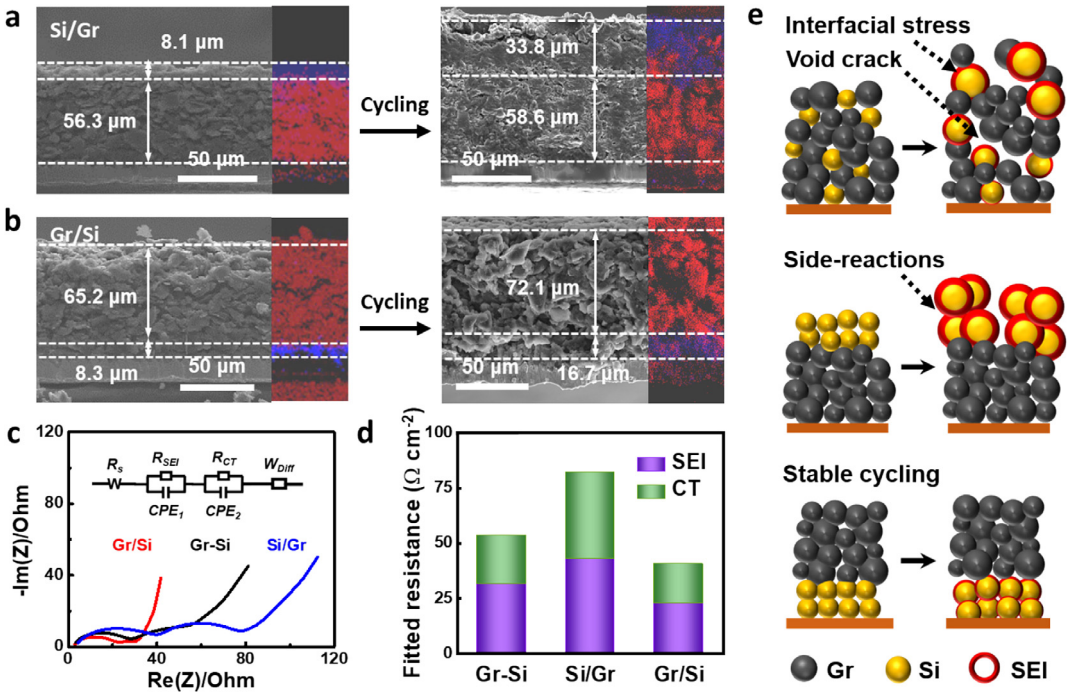

Fig. 4. Cross-section SEM and EDS elemental mapping images of (a) layered Si/Gr and (b) layered Gr/Si electrodes before and after cycling (the Si and C elements are displayed by blue and red, respectively). (c) EIS and (d) fitted resistance results of the conventional Gr-Si, layered Si/Gr, and layered Gr/Si electrodes after cycling. The layered Gr/Si electrode showed the smallest resistance. (e) The schematic of the failure mechanism of the conventional Gr-Si and layered Si/Gr electrodes, and the stable cycling performance of the layered Gr/Si electrode.

Encouraged by the stable structural and electrochemical properties of layered Gr/Si electrode, the cycling performance of the Gr-Si hybrid anodes was tested with an increased Si loading of 17 wt%. As shown in Fig. S16, the layered Gr/Si electrode showed a high initial capacity of 690.5 mA h g^{-1}, which maintained 94.4% after 100 cycles at 0.2 *C* in half cells. In contrast, the conventional Gr-Si electrode and layered Si/Gr electrode showed low capacities of 307.3 and 458.6 mA h g^{-1} after the same 100 cycles. Besides, the ACE of the layered Gr/Si electrode reached 99.2%, higher than the conventional Gr-Si (98.9%) and layered Si/Gr (99.0%). The significance of constructing layered electrode structure in improving Gr-Si hybrid anodes was further verified by using another two types of Si sources, namely Si nanospheres (nanoSi, Fig. S17) and Si oxide particles (SiO_x, Fig. S18). As shown in the Fig. S19, the layered Gr/nano-Si electrode showed the highest capacity retention of 83.0% after 100 cycles at 0.2 *C*, outperformed the layered nanoSi/Gr electrode (49.1%) and conventional Gr-nanoSi electrode (31.2%) under the same test condition. Meanwhile, the layered Gr/SiO_x electrode showed the highest capacity retention of 98.3% after 100 cycles at 0.2 *C*, outperformed the layered SiO_x/Gr electrode (67.8%) and conventional Gr-SiO_x electrode (63.4%) under the same test condition (Fig. S20). It is noteworthy, based on our empirical observations, that the oxidation of silicon influences the cycling stability of this active material, as SiO_x undergoes a reduced volumetric change in comparison to Si during the lithiation/delithiation processes. In pursuit of higher cycling stability, we employed SiO_x instead of Si to prepare layered Gr-Si electrode with the same Si loading of 17 wt%, and further examined it in pouch cells with commercial $LiNi_{0.6}Co_{0.2}Mn_{0.2}O_2$ (NCM622) cathodes and a low N/P ratio of 1.09 (Fig. 5a). As demonstrated in Fig. 5b–d, the layered Gr/SiO_x-based pouch cell showed a high capacity of 283 mA h, a stable charge/discharge cycling with a high capacity retention of 91.6% and a high ACE of 99.9% after 200 cycles at the low rate of 0.3 *C*, superior to the hybrid Gr-SiO_x counterpart (capacity retention: 49.4%, ACE: 99.3%), further suggesting the excellent cycling stability of the layered Gr/SiO_x electrode. More impressively, the practicality of as-designed layered Gr/SiO_x anode was evaluated in an Ah-level pouch cell (Fig. 5e), which displayed a high capacity retention of 94.5% after 100 charge/discharge cycles at 0.3 *C* (Fig. 5f). Noted that the capacity decay rate of the Ah-level layered Gr/SiO_x-based pouch cell was as low as 0.0546% per cycle, outperforming most Gr-Si hybrid electrodes in recent publications (Fig. 5g, Table S2).

4. Conclusions

In summary, we advocate the design of layered electrode structure design (Gr/Si) as a potent strategy to tackle the mechano-electrochemical instability inherent in Gr-Si hybrid anodes. In the case of conventional Gr-Si electrodes, the significant volume change of Si particles exerted local stress to Gr, culminating in capacity fading of Gr materials. Furthermore, the different volume change ratio between Si and Gr particles instigated the formation of porous electrode and the increased charge transfer during battery cycling. Therefore, the layered Gr/Si electrode with the minimal Si/Gr interface and the most stable electrode structure showed the best cycling stability with a high capacity retention of 94.4% after 100 cycles at 0.2 *C* in half cell configuration. Moreover, the layered Gr/Si electrode, boasting a high photovoltaic waste Si loading of 17 wt%, fostered excellent electrochemical cycling stability in an Ah-level layered Gr/Si-based full pouch cell with a low N/P ratio of 1.09. It demonstrated a significantly low capacity decay rate of 0.0546% per cycle at 0.3 *C*, superior to most high-performance Gr-Si hybrid anodes in recent publications. In addition, it is expected that the replacement of photovoltaic waste Si with high-performance commercial Si active material to prepare layered Gr/Si electrodes would help further performance breakthroughs for future researches. This work not only illuminates the mechano-electrochemical instability issue of conventional Gr-Si hybrid electrodes, but also offers a novel perspective on the

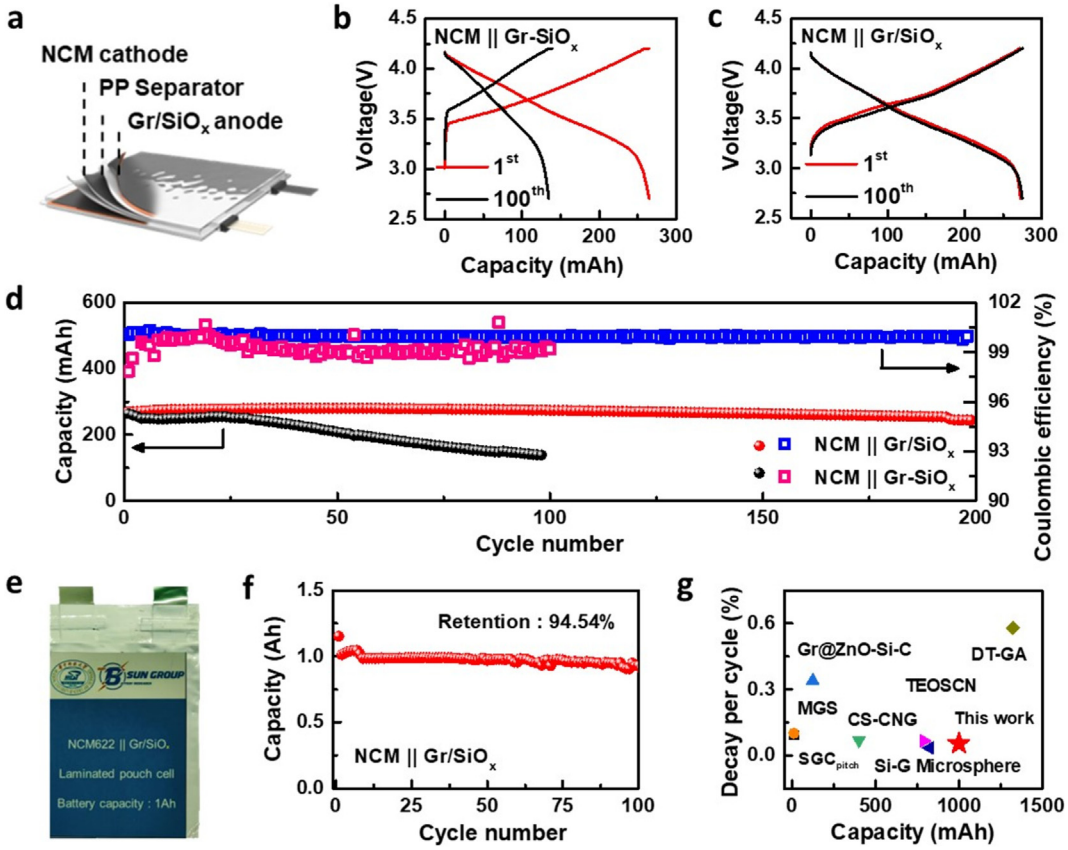

Fig. 5. (a) Configuration of the as-assembled pouch cells with layered Gr/SiO_x anode and commercial NCM cathode. Charge and discharge curves of (b) the conventional Gr-SiO_x||NCM and (c) layered Gr/SiO_x||NCM pouch cells at 0.3 *C* for the 1st and 100th cycles. (d) Cycling performance and Coulombic efficiency of conventional Gr-SiO_x||NCM and layered Gr/SiO_x||NCM pouch cells at 0.3 *C*. (e) Digital image and (f) cycling performance of an Ah-level layered Gr/SiO_x||NCM pouch cell at 0.3 *C*. (g) Comparison of the capacity decay rates between as-designed layered Gr/SiO_x electrode and the high-performance Si-Gr hybrid anodes in recent reports. (For more details please see Table S2).

development of advanced Gr-Si hybrid anodes by meticulous electrode structure design.

Author contributions

C. Li, **L. Wang**, and **Y. Sun** conceived the idea. **C. Li**, **X. Wang**, **Z. Cai**, **R. Zhan**, **X. Duan**, **X. Liu**, and **K. Cheng** performed the experiments. **J. Wang** and **Z. Cai** conducted the first principles calculation. **C. Li**, **Z. Cai**, **L. Wang**, and **Y. Sun** wrote the manuscript. **Z. Cai**, **L. Wang**, and **Y. Sun** supervised the project. All authors contributed to the discussion and provided feedback on the manuscript.

CRediT authorship contribution statement

Chunhao Li: Writing – original draft, Methodology, Investigation, Data curation. **Jing Wang:** Methodology. **Xiancheng Wang:** Data curation. **Zihe Chen:** Data curation. **Renming Zhan:** Data curation. **Xiangrui Duan:** Data curation. **Xuerui Liu:** Data curation. **Kai Cheng:** Data curation. **Zhao Cai:** Writing – review & editing, Supervision, Methodology, Data curation. **Li Wang:** Writing – review & editing, Supervision. **Yongming Sun:** Writing – review & editing, Supervision, Conceptualization.

Declaration of competing interest

The authors declare that they have no known competing financial interests or personal relationships that could have appeared to influence the work reported in this paper.

Acknowledgements

Y. Sun acknowledges the financial support by the National Natural Science Foundation of China (52072137). Z. Cai acknowledges the National Natural Science Foundation of China (22205068) and the "CUG Scholar" Scientific Research Funds at China University of Geosciences (Wuhan) (2022118). The authors would like to thank the Analytical and Testing Center of Huazhong University of Science and Technology as well as the Center for Nanoscale Characterization & Devices of Wuhan National Laboratory for Optoelectronics for providing the facilities to conduct the characterization.

Appendix A. Supplementary material

Supplementary material to this article can be found online at https://doi.org/10.1016/j.jechem.2024.12.048.

References

[1] Z. Zhao, F. Chen, J. Han, D. Kong, S. Pan, J. Xiao, S. Wu, Q.H. Yang, Adv. Energy Mater. 13 (2023) 2300367.
[2] X. Liu, Y. Tan, W. Wang, C. Li, Z.W. Seh, L. Wang, Y. Sun, Nano Lett. 20 (2020) 4558–4565.
[3] B.S. Lee, S.-H. Oh, Y.J. Choi, M.-J. Yi, S.H. Kim, S.-Y. Kim, Y.-E. Sung, S.Y. Shin, Y. Lee, S.-H. Yu, Nat. Commun. 14 (2023) 150.
[4] S. Tu, B. Zhang, Y. Zhang, Z. Chen, X. Wang, R. Zhan, Y. Ou, W. Wang, X. Liu, X. Duan, L. Wang, Y. Sun, Nat. Energy. 8 (2023) 1365–1374.
[5] J. Du, W. Wang, M. Wan, X. Wang, G. Li, Y. Tan, C. Li, S. Tu, Y. Sun, Adv. Energy Mater. 11 (2021) 2102259.
[6] Y. Cui, Nat. Energy 6 (2021) 995–996.
[7] F. Aupperle, G.G. Eshetu, K.W. Eberman, A. Xioa, J.-S. Bridel, E. Figgemeier, J. Mater. Chem. A 8 (2020) 19573–19587.

[8] P. Li, H. Kim, S.-T. Myung, Y.-K. Sun, Energy Storage Mater. 35 (2021) 550–576.
[9] K. Richter, T. Waldmann, N. Paul, N. Jobst, R.G. Scurtu, M. Hofmann, R. Gilles, M. Wohlfahrt-Mehrens, ChemSusChem 13 (2020) 529–538.
[10] S. Chae, S.H. Choi, N. Kim, J. Sung, J. Cho, Angew. Chem. Int. Ed. 59 (2020) 110–135.
[11] Z. Cai, J. Wang, Y. Sun, eScience 3 (2023) 100093.
[12] X. Li, P. Yan, X. Xiao, J.H. Woo, C. Wang, J. Liu, J.-G. Zhang, Energy Environ. Sci. 10 (2017) 1427–1434.
[13] M. Ko, S. Chae, J. Ma, N. Kim, H.-W. Lee, Y. Cui, J. Cho, Nat. Energy 1 (2016) 16113.
[14] N. Kim, S. Chae, J. Ma, M. Ko, J. Cho, Nat. Commun. 8 (2017) 812.
[15] S.-H. Choi, G. Nam, S. Chae, D. Kim, N. Kim, W.S. Kim, J. Ma, J. Sung, S.M. Han, M. Ko, H.-W. Lee, J. Cho, Adv. Energy Mater. 9 (2019) 1803121.
[16] J. Ma, J. Sung, J. Hong, S. Chae, N. Kim, S.H. Choi, G. Nam, Y. Son, S.Y. Kim, M. Ko, J. Cho, Nat. Commun. 10 (2019) 475.
[17] J. Ma, J. Sung, Y. Lee, Y. Son, S. Chae, N. Kim, S.H. Choi, J. Cho, Adv. Energy Mater. 10 (2019) 1903400.
[18] S. Chae, N. Kim, J. Ma, J. Cho, M. Ko, Adv. Energy Mater. 7 (2017) 1700071.
[19] S.-Y. Lim, Solid State Sci. 93 (2019) 24–30.
[20] T. Lee, N. Kim, J. Lee, Y. Lee, J. Sung, H. Kim, S. Chae, H. Cha, Y. Son, S.K. Kwak, J. Cho, Adv. Energy Mater. 13 (2023) 2301139.
[21] W. Liu, Y. Zhong, S. Yang, S. Zhang, X. Yu, H. Wang, Q. Li, J. Li, X. Cai, Y. Fang, Sustain. Energy Fuel 2 (2018) 679–687.
[22] Z. Yi, W. Wang, Y. Qian, X. Liu, N. Lin, Y. Qian, A.C.S. Sustain, Chem. Eng. 6 (2018) 14230–14238.
[23] P. Li, J.Y. Hwang, Y.K. Sun, ACS Nano 13 (2019) 2624–2633.
[24] G. Nava, J. Schwan, M.G. Boebinger, M.T. McDowell, L. Mangolini, Nano Lett. 19 (2019) 7236–7245.
[25] J. Li, Y. Huang, W. Huang, J. Tao, F. Lv, R. Ye, Y. Lin, Y.Y. Li, Z. Huang, J. Lu, Small 17 (2021) 2006373.
[26] X. Liu, H. Liu, Y. Cao, X. Wu, Z. Shan, ACS Appl. Mater. Interfaces 15 (2023) 9457–9464.
[27] G. Ge, G. Li, X. Wang, X. Chen, L. Fu, X. Liu, E. Mao, J. Liu, X. Yang, C. Qian, Y. Sun, Nano Lett. 21 (2021) 3127–3133.
[28] G. Zheng, Y. Xiang, L. Xu, H. Luo, B. Wang, Y. Liu, X. Han, W. Zhao, S. Chen, H. Chen, Q. Zhang, T. Zhu, Y. Yang, Adv. Energy Mater. 8 (2018) 1801718.
[29] L. Hu, X. Zhang, P. Zhao, H. Fan, Z. Zhang, J. Deng, G. Ungar, J. Song, Adv. Mater. 33 (2021) 2104416.
[30] J. Kim, J. Choi, K. Park, S. Kim, K.W. Nam, K. Char, J.W. Choi, Adv. Energy Mater. 12 (2022) 2103718.
[31] J. Xiong, N. Dupré, P. Moreau, B. Lestriez, Adv. Energy Mater. 12 (2022) 2103348.
[32] C. Kang, Y.W. Cho, J. Power Sources 485 (2021) 229311.
[33] K.P.C. Yao, J.S. Okasinski, K. Kalaga, J.D. Almer, D.P. Abraham, Adv. Energy Mater. 9 (2019) 1803380.
[34] Y. Xiong, Y. Liu, L. Chen, S. Zhang, X. Zhu, T. Shen, D. Ren, X. He, J. Qiu, L. Wang, Q. Hu, H. Zhang, Energy Environ. Mater. 5 (2022) 872–876.
[35] Y. Zhang, Z. Wang, K. Hu, J. Ren, N. Yu, X. Liu, G. Wu, N. Liu, Energy Storage Mater. 34 (2021) 311–319.
[36] H. Shin, Y.K. Lee, W. Lu, J. Power Sources 528 (2022) 231223.
[37] J. Moon, H.C. Lee, H. Jung, S. Wakita, S. Cho, J. Yoon, J. Lee, A. Ueda, B. Choi, S. Lee, K. Ito, Y. Kubo, A.C. Lim, J.G. Seo, J. Yoo, S. Lee, Y. Ham, W. Baek, Y.G. Ryu, I. T. Han, Nat. Commun. 12 (2021) 2714.
[38] C. Li, Y. Zhu, Y. Quan, F. Zong, J. Wang, D. Zhao, N. Zhang, P. Wang, X. Cui, S. Li, J. Energy. Chem. 98 (2024) 680–691.
[39] L. Song, S. Li, J. Wang, J. Zhu, Y. Wang, X. Cai, F. Zong, H. Wang, X. Cui, D. Zhao, ACS Appl. Mater. Interfaces 15 (2023) 49727–49738.
[40] E. Moyassari, T. Roth, S. Kücher, C.-C. Chang, S.-C. Hou, F.B. Spingler, A. Jossen, J. Electrochem. Soc. 169 (2022) 010504.
[41] C.L. Berhaut, M. Mirolo, D.Z. Dominguez, I. Martens, S. Pouget, N. Herlin-Boime, M. Chandesris, S. Tardif, J. Drnec, S. Lyonnard, Adv. Energy Mater. 13 (2023) 2301874.
[42] G. Qian, Y. Li, H. Chen, L. Xie, T. Liu, N. Yang, Y. Song, C. Lin, J. Cheng, N. Nakashima, M. Zhang, Z. Li, W. Zhao, X. Yang, H. Lin, X. Lu, L. Yang, H. Li, K. Amine, L. Chen, F. Pan, Nat. Commun. 14 (2023) 6048.